Project acronym and title:
SECURe – Subsurface Evaluation of Carbon capture and storage and Unconventional risks

D5.8 REPORT ON KINETICS OF ENHANCED CEMENTATION REACTIONS FOR CO_2 LEAKAGE REMEDIATION AND FAULT HEALING PROCESSES

Authors and affiliation:
Yukun Ji[1] and Veerle Vandeginste[2]

[1]School of Chemistry, University of Nottingham, Nottingham, NG7 2RD, United Kingdom

[2]KU Leuven Campus Bruges, Department of Materials Engineering, Bruges, B-8200, Belgium

Email of lead author:
yukun.ji1@nottingham.ac.uk

D5.8
Revision:1

Project funded by the European Commission within the Horizon 2020 Programme		
Dissemination Level		
PU	*Public*	*X*

Deliverable number:	**5.8**
Deliverable name:	**REPORT ON KINETICS OF ENHANCED CEMENTATION REACTIONS FOR CO2 LEAKAGE REMEDIATION AND FAULT HEALING PROCESSES**
Work package:	**WP5 Impact Mitigation and Remediation**
Lead WP/deliverable beneficiary:	WP5 (University of Nottingham)

Status of deliverable		
	By	**Date**
Submitted (Author(s))	**Yukun Ji and Veerle Vandeginste**	**22.02.2021**
Verified (WP leader)	Pierre Cerasi	
Approved (EB member)	Jens Wollenweber/Elisa Calignano (TNO)	**23.02.2021**
Approved (Coordinator)	E HOUGH	26.02.2021

Author(s)		
Name	**Organisation**	**E-mail**
Yukun Ji	**University of Nottingham**	**yukun.ji1@nottingham.ac.uk**
Veerle Vandeginste	**KU Leuven Campus Bruges**	**veerle.vandeginste@kuleuven.be**

Public introduction

Subsurface Evaluation of CCS and Unconventional Risks (SECURe) is gathering unbiased, impartial scientific evidence for risk mitigation and monitoring for environmental protection to underpin subsurface geoenergy development. The main outputs of SECURe comprise recommendations for best practice for unconventional hydrocarbon production and geological CO_2 storage. The project is funded from June 2018–May 2021.

The project is developing monitoring and mitigation strategies for the full geoenergy project lifecycle; by assessing plausible hazards and monitoring associated environmental risks. This is achieved through a program of experimental research and advanced technology development that includes demonstration at commercial and research facilities to formulate best practice. We will meet stakeholder needs; from the design of monitoring and mitigation strategies relevant to operators and regulators, to developing communication strategies to provide a greater level of understanding of the potential impacts.

The SECURe partnership comprises major research and commercial organisations from countries that host shale gas and CCS industries at different stages of operation (from permitted to closed). We are forming a durable international partnership with non-European groups; providing international access to study sites, creating links between projects and increasing our collective capability through exchange of scientific staff.

Executive report summary

The precipitation of acid-resistant carbonate minerals through chemical interaction between injected fluids and leaking CO_2 can act as an effective sealant for remediating CO_2 leakage through faults and fractures in geologic CO_2 storage reservoirs. Magnesite is one of the most stable carbonate phases that can contribute to addressing the challenge of long term plugging of CO_2 leakage, and the chemical mechanism that can catalyse its formation is of great interest and practical significance. Here, using batch reactor experiments and mineralogical characterization, we explored magnesite precipitation kinetics in chemically complex fluids whereby the impact of fluid acidity and alkalinity, NaCl, and MgO nanoparticles was investigated. The results show that the addition of NaOH or of NaCl to the fluid significantly accelerates magnesite formation by enhanced phase transition of hydrated metastable magnesium carbonate to magnesite. Raised CO_3^{2-} activity in an alkaline environment may promote the transformation of hydromagnesite into magnesite. A competition for hydration water between the background ions and magnesite building ions in the presence of NaCl can promote Mg dehydration and magnesite mineralization. Although the hydrophilic nature of MgO may retard magnesite formation at the early stage of the reaction, an alkaline pH environment can subsequently accelerate magnesite growth by enhanced replacement of hydromagnesite. This research provides new insights into the mechanism and kinetics of magnesite formation at mineral-fluid interfaces in a range of conditions, and can help facilitate defining strategies to mitigate risks involved with underground CO_2 leakage.

Contents

FIGURES

TABLES

1 Introduction

Carbon sequestration through underground storage of captured CO_2 in deep geologic reservoirs is an efficient way to control global warming (Lackner, 2003), whereas potential CO_2 leakage pathways including geological faults, high permeability zones, and fractures have led to a considerable concern (Castaneda-Herrera et al., 2018; Kim et al., 2019). CO_2 leakage and/or brine coming from CO_2 geological storage sites can pose a risk for overlying fresh groundwater resource, resulting in a low pH, variation in redox potential, change of microbial metabolism, and potential contaminant mobilisation (Lions et al., 2014). Moreover, high CO_2 concentrations and long term exposure in air could augment adverse consequences to human health (Benson et al., 2002). Specific procedures for mitigating and remediating CO_2 leakage should be proposed to control CO_2 leakage induced potential environmental and climate change issues.

Mineral precipitates produced through the chemical reaction between remediation fluids and leaking CO_2 can fill up and plug pores or open fractures of a high permeability zone (e.g. calcium hydroxide could generate a pore blocking-carbonate mineral in contact with CO_2) (Ito et al., 2006; Brydie et al., 2014), thus blocking the leakage pathways. Natural rocks have narrow pores and fractures, and aqueous solutions with low viscosity that can pass through small pores are treated as a more promising reactive grouting fluid (Ito et al., 2014). However, the plugging induced CO_2 accumulation at the repaired zone can result in a decrease in pore water pH, and thus may drive the gradual dissolution of calcium carbonate ($CaCO_3$) (Ito et al., 2014). Hence, more stable reaction products under a CO_2 leakage scenario (slightly acidic environment) can act as a long term effective sealant, and thus have potential to reduce pore volume and pore connectivity. The acid-resistant precipitates that can effectively block CO_2 leakage mitigate risks involved with underground CO_2 storage and offer solutions for remediation of fractures. Magnesite ($MgCO_3$) can be treated as a more acid-resistant mineral compared to calcite in acidic scenarios (Palandri and Kharaka, 2004). In addition, the magnesite dissolution rate is 100-1000 times lower than that of calcite under an ambient temperature of 150 °C and pH range of 1 to 14 (Pokrovski et al., 2009). Multiple metastable hydrated magnesium carbonates (e.g. $MgCO_3 \cdot 3H_2O$, $MgCO_3 \cdot 5H_2O$, and $(MgCO_3)_4 \cdot Mg(OH)_2 \cdot 4H_2O$ precede magnesite precipitation (Hänchen et al., 2008), and the formation of anhydrous magnesite is kinetically inhibited (Königsberger et al., 1999). Generally, hydrated magnesium carbonates are more soluble and less stable than anhydrous magnesite, and magnesite is the most stable form of magnesium carbonate and it has the potential for long-term CO_2 storage (Power et al., 2013). Hence, magnesite precipitation is investigated in mineral-fluid interaction studies with aqueous systems saturated with CO_2.

Notably, the formation of anhydrous magnesite is kinetically inhibited (Königsberger et al., 1999). The difficulty in anhydrous magnesite formation is mainly attributed to the strong hydration nature of magnesium ions (e.g. Deelman, 2001) and high energy barrier for forming long-range ordered crystallographic structures (Xu et al., 2013). Magnesium ions can bind with six water molecules to form a complex ($[Mg(H_2O)_6]^{2+}$) in an octahedral structure, and the strong association of magnesium ions with water is due to the high charge density of magnesium ions related to the small ionic radius (0.65 Å) (Allnér et al., 2012). The slower precipitation rate of magnesite compared to calcite is attributed to the much slower water exchange rate and higher dehydration enthalpy for magnesium ions in comparison to calcium ions (Saldi et al., 2009; Yang et al., 2012; Bracco et al., 2014). Hence, water dehydration around the magnesium ion may act as an important factor for magnesite formation. Elevated temperature favours the dehydration of the magnesium ions for their integration into the magnesite crystal (Sayles and Fyfe, 1973). Furthermore, a higher precipitation rate of magnesite is expected at higher temperature (>100 °C) and CO_2 partial pressure (~100 bar) conditions (Hänchen et al., 2008). Saline environments can decrease the water activity and result in the dehydration of the magnesium ions (Christ and Hostetler, 1970), thereby potentially causing a positive impact on the reaction pathway and kinetic growth of magnesite. Furthermore, alkaline scenarios can potentially provide a favorable condition for carbonate formation since carbon speciation increases in the order of $CO_2 < HCO_3^- < CO_3^{2-}$ under alkaline scenarios and increased CO_3^{2-} activity can increase the carbonate mineral saturation index. Moreover, it has been reported that sulfate reducing bacteria can increase the alkalinity by reducing sulfate ions and consuming organic acids,

and thus playing a critical role in calcium carbonate precipitation (Braissant et al., 2007). The death and decay of algae could release ammonia and create an alkaline pH environment, thus favoring magnesite formation (Valdiya, 1968). Thompson and Ferris (1990) further indicated that magnesite biomineralization could be occurring in high pH (8.5-10.0) aquatic environments rich in magnesium. Furthermore, heterogeneous nucleation is also a possible way which can enable faster precipitation through reducing the activation energy barrier of nucleation (e.g. Sear, 2006; Atashin et al., 2017), and it has been verified that $MgCO_3$ seeding can accelerate the growth of anhydrous magnesite (Swanson et al., 2014).

In order to achieve an effective leakage remediation, the remediation fluids should be injected into targeted zones above the caprock layer for remediating leakage through faults and fractures (Ito et al., 2014; Mosleh et al., 2017). The remediation fluids will be injected into the fractures and rocks through boreholes. How to manipulate injection rate of remediation fluid is also an important factor that could influence CO_2 leakage remediation. It is noted that this study focuses on the kinetics of anhydrous magnesite precipitation by reacting $MgCl_2$ with Na_2CO_3 fluids under various conditions (acidity, alkalinity, background electrolyte, and use of MgO nanoparticles) in batch reactor experiments. This research enables new insights into the mechanism and kinetics of anhydrous magnesite precipitation (through the replacement of hydrated metastable magnesium carbonate by anhydrous magnesite) under different conditions, and thus provides researchers effective chemical solutions for effective leakage remediation under specific geologic conditions. Moreover, our results can further provide a better understanding of the fundamental chemistry underlying the application of carbon storage through mineralization.

2 Methodology

2.1 MATERIALS AND BATCH REACTOR EXPERIMENTS

The remediation fluid and carbon source were simulated by $MgCl_2$ and Na_2CO_3 solutions in this study. $MgCl_2$, Na_2CO_3, NaCl, HCl, and NaOH used in this study are of analytic reagent grade. Aqueous solutions of $MgCl_2$ and Na_2CO_3 were prepared with milli-Q water. The control experiments were conducted with 15 mL of simulated fluids containing 0.3 M $MgCl_2$ and 0.3 M Na_2CO_3, in Teflon-lined steel batch reactors. The acidity, alkalinity, background electrolytes, and hydrophilic particles influenced experiments were conducted using HCl (10^{-5} M), NaOH (10^{-5} M), NaCl (0.5, 1.0, 1.5, 2.0 M), and MgO nanoparticles (40-60 nm) (6, 12, 18, 24 mg) to test different fluid compositions for magnesite formation, respectively (Table 1). Experiments at the same NaOH concentration as HCl concentration were carried out to make a comparison with slightly acidic environment influenced experiments. A temperature of 200 °C was applied for the experiments to generate anhydrous magnesite at favorable time scales for laboratory experiment. Depending on local geothermal gradients, the temperature at the initial emplacement zone of supercritical CO_2 could reach up to 150-200 °C (e.g. Kaszuba et al., 2003). Future research will involve testing the effect of fluid compositions on the rate of magnesium carbonate formation at low temperature. The fluids in the experiments were mixed at room temperature (for safety reasons) in Teflon-lined steel batch reactors just before being placed in a pre-heated oven at 200 °C. Given our experiments have the same temperature conditions and same experimental procedures, we can compare the impact of fluid conditions on magnesite precipitation. Five series of batch reactor experiments were carried out whereby samples were taken every 1 h over a total time of 7 h, and all experiments in this study were duplicated. Centrifuge tubes were used to collect the reaction products from the batch reactor experiments, and the pH of the supernatant solution after centrifugation (5 min at 4500 rpm) was tested using a pH meter. Furthermore, the reaction products were subsequently cleaned two times with milli-Q water, and the liquids were then decanted after high speed centrifugation for 5 min (4500 rpm). The residue solid was dried in a drying oven at 50 °C and stored in plastic flasks for XRD characterization, and the weight of the reaction products was subsequently recorded.

2.2 METHODS

The reaction products were analysed by X-ray diffraction (XRD) to identify the mineralogical composition. Bulk sample powders were scanned over a sampling range of 2 to 70 °2θ with a step size of 0.0131 and a scan speed of 0.082 °2θ per second, and a PANalytical X'Pert Pro was applied for these analyses by using Cu K-α radiation at 40 kV and 40 mA. The phase identification was accomplished by comparison with reference spectra in a database. The relative ratios of magnesite and metastable hydrated magnesium carbonate were calculated based on the ratio of respective main peak areas. Analysis of the peak intensities on the sample X-ray diffractograms enable quantitative evaluation (using DIFFRAC. EVA-XRD software) of the amount of different mineralogical components. The mineralogical compositions of the samples taken at one hour time steps in the different experimental series are shown in supplementary material (Table A.1-22).

Table 1 Summary of experiments

Variable	No.	HCl (mol/L)	NaOH (mol/L)	NaCl (mol/L)	MgO (mg)	$MgCl_2$ (mol/L)	Na_2CO_3 (mol/L)	Temperature (°C)
control	1	0	0	0	0	0.3	0.3	200
acidity	2	10^{-5}	0	0	0	0.3	0.3	200
alkalinity	3	0	10^{-5}	0	0	0.3	0.3	200
NaCl	4	0	0	0.5	0	0.3	0.3	200
	5	0	0	1.0	0	0.3	0.3	200
	6	0	0	1.5	0	0.3	0.3	200
	7	0	0	2.0	0	0.3	0.3	200
MgO (40-60 nm)	8	0	0	0	6	0.3	0.3	200
	9	0	0	0	12	0.3	0.3	200
	10	0	0	0	18	0.3	0.3	200
	11	0	0	0	24	0.3	0.3	200

3 Results

3.1 ACIDITY AND ALKALINITY EFFECTS

Metastable magnesium carbonate is formed upon mixing the Mg-rich fluids with carbon-rich fluid at room temperature, and is then followed by conversion to anhydrous magnesite at the high temperature conditions (200 °C) of the laboratory experiments. No anhydrous magnesite was detected in control experiments at one hour reaction time based on detailed powder X-ray diffractogram analysis. Instead, approximately 40% hydromagnesite ($(MgCO_3)_4 \cdot Mg(OH)_2 \cdot 4H_2O$) (Table A.1) was formed from solutions of $MgCl_2$ and Na_2CO_3. Moreover, oxymagnesite ($MgO \cdot 2MgCO_3$) (approximately 60%) was detected after 1 h and it was identified in the reaction products based on its XRD pattern (Fig. 1; Table A.1). At 2 hours of reaction time, a composition of magnesite (55%), hydromagnesite (19%), and oxymagnesite (26%) was observed in control experiments (Table A.1 and A.2). The relative amount of hydromagnesite and oxymagnesite decreases with reaction time and these minerals are simultaneously replaced by anhydrous magnesite (e.g. Fig. 1 and 2). The XRD results show that metastable magnesium carbonates have almost disappeared (Table A.1 and Fig. 3a) within four hours reaction time and magnesite is the dominant reaction product. Furthermore, a small amount of brucite can be identified at the end of experiments (Table A.1).

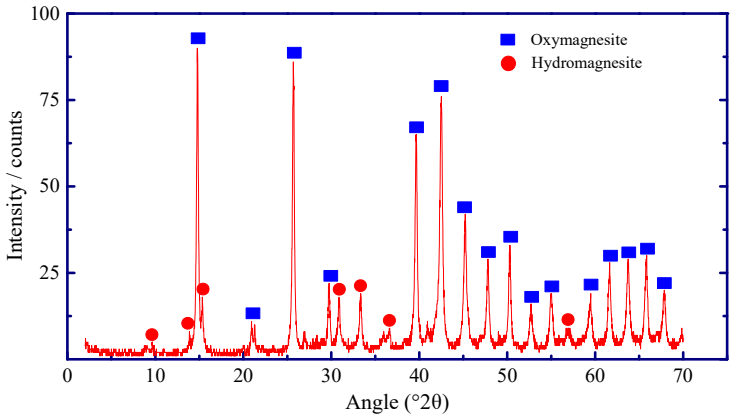

Fig. 1. X-ray diffractogram of reaction products in the control experiment at one hour reaction time.

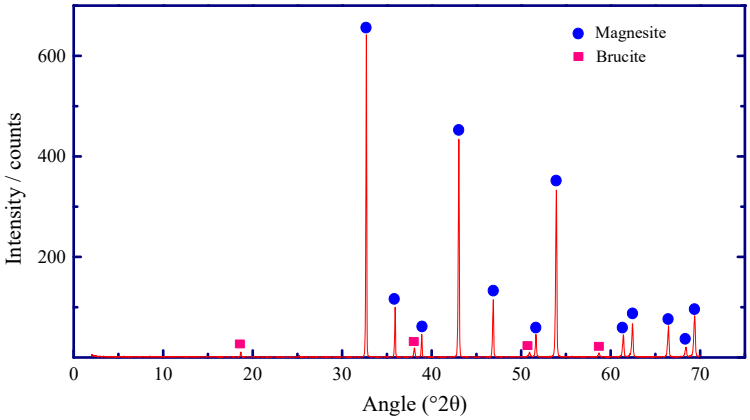

Fig. 2. X-ray diffractogram of reaction products in the control experiment at six hours reaction time.

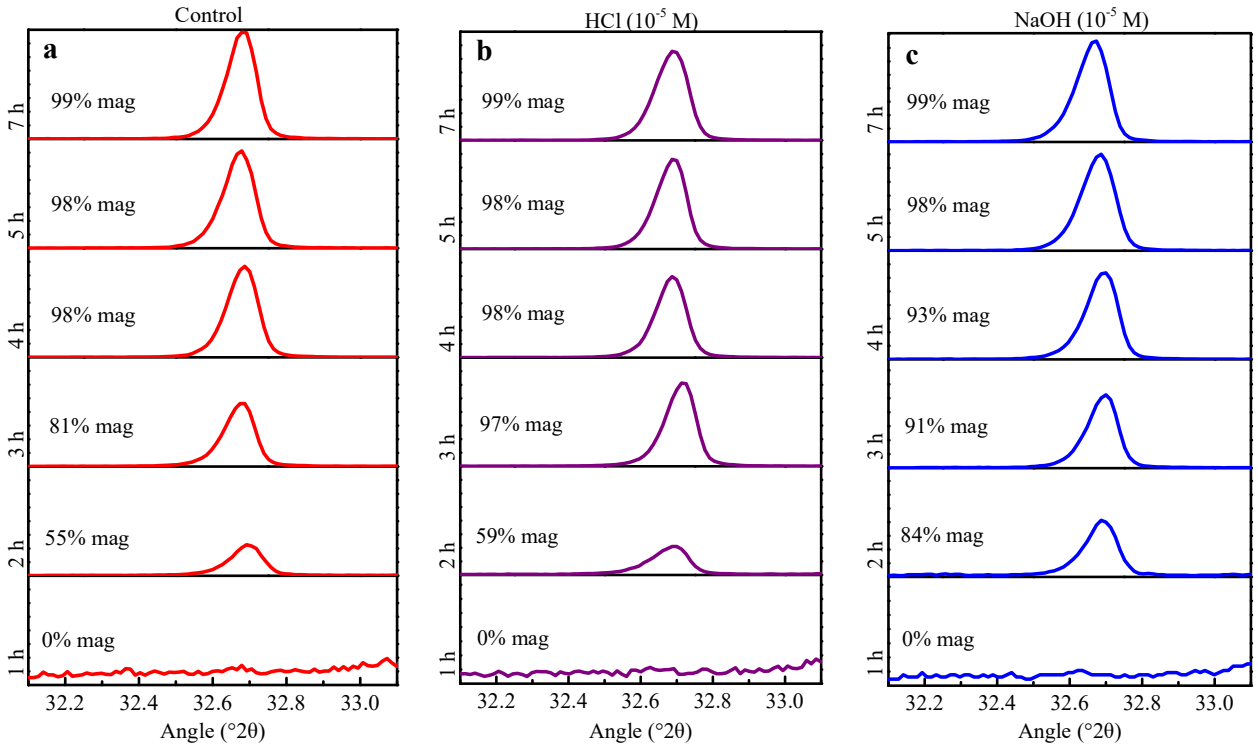

Fig. 3. Powder X-ray diffractogram selected area (32.1-33.1 °2θ) of reaction products. The crystallographic data of the reaction products: (a) control experiment; (b) 10^{-5} M HCl experiments; (c) 10^{-5} M NaOH experiments. The % mag refers to the percentage of magnesite as calculated from the main magnesite peak.

In HCl experiments, both hydromagnesite and oxymagnesite were observed at one hour reaction time, but no anhydrous magnesite (Table A.3). The average hydromagnesite content at one hour reaction time in HCl experiments (59%) is significantly higher than that in control experiments (40%). Moreover, the kinetics of magnesite formation were slightly accelerated compared to control experiments (Fig. 3a and 3b). At two hours reaction time, the transformed magnesite in HCl experiments ($0.196\pm4.0\times10^{-3}$ g) was slightly higher than that in control experiments ($0.180\pm5.6\times10^{-3}$ g) (Table A.1-4). By addition of H^+ ions into $MgCl_2$-Na_2CO_3 aqueous solutions, the average magnesite content of HCl experiments at three hours reaction time is significantly higher than the average magnesite content of control experiments (Fig. 4). These results demonstrate that an increase in kinetic replacement of magnesite could be driven by H^+ ions in solution (Table A.3; Fig. 4). Based on the NaOH experiments, it was found that NaOH played a catalytic role for hydromagnesite and magnesite formation (e.g. Table A.1 and A.5). A higher hydromagnesite content (57%) was observed at one hour reaction time compared to hydromagnesite content in control experiments (40%). Phase transition from metastable intermediates to magnesite was significantly facilitated in an alkaline scenario compared to control experiments (Table A.1 and A.5), and magnesite formation occurred rapidly within two hours reaction time for experiments with 10^{-5} M NaOH (Fig. 3a and 3c). An increase of 29% magnesite content in comparison to the control experiments can be observed at two hours reaction time (Fig. 4), and the respectively transformed magnesite was $0.289\pm1.1\times10^{-2}$ g and $0.180\pm5.6\times10^{-3}$ g.

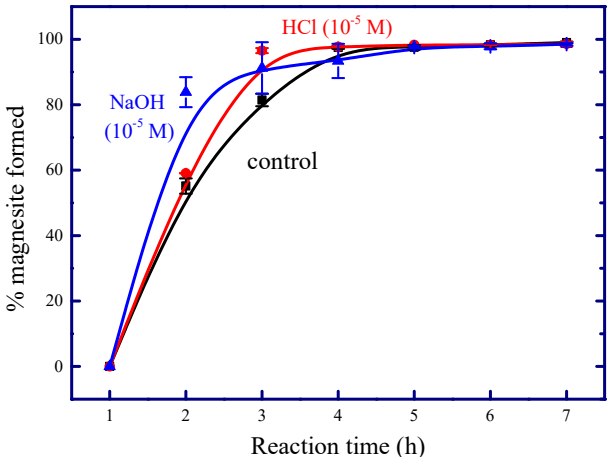

Fig. 4. Magnesite formation reaction curves under control, slight acidity and alkalinity conditions. Error bars represent standard deviation of measurements from duplicate experiments.

3.2 NaCl EFFECTS

The addition of 2.0 M NaCl to the $MgCl_2$-Na_2CO_3 fluids can accelerate the formation of magnesite. Besides hydromagnesite and oxymagnesite, up to 27% of reaction solids is anhydrous magnesite at 1 h reaction time (Fig. 5). This suggests a significantly higher formation rate of magnesite in the presence of background electrolyte (2.0 M NaCl). From the first hour to the second hour of the reaction, $0.115\pm5.1\times10^{-4}$ g of hydromagnesite was transformed into magnesite in 0.5 M NaCl experiments compared to $0.0596\pm2.6\times10^{-4}$ g transformed hydromagnesite in control experiments. This indicates that the conversion of hydromagnesite into magnesite is catalysed in the presence of NaCl. At two hours reaction time, the highest relative percentage of magnesite (95%) in the reaction solids was also found in the experiments with 2.0 M NaCl (Fig. 5; Table A.13-14). The addition of NaCl in the fluids means an increase in the ionic strength of the solutions. Furthermore, the magnesite percentage continuously increases from 85% to 95% with the increase of NaCl concentration from 0.5 M to 2.0 M at 2 hours reaction time (Fig. 6; Table A.7-14). This implies that higher ionic strength is correlated with increased magnesite content.

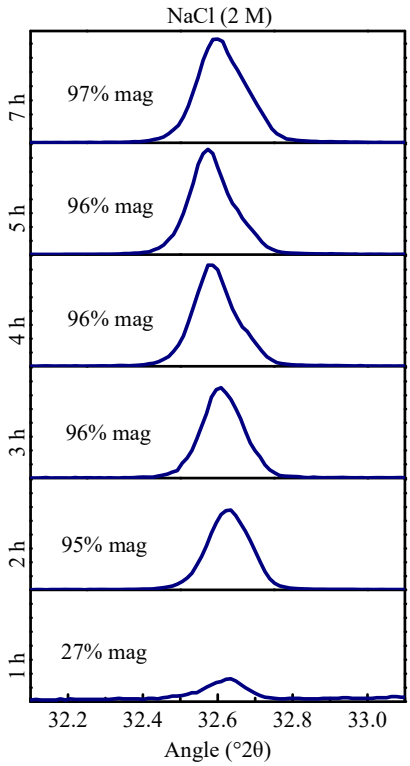

Fig. 5. Magnesite formation reaction curves under control, slight acidity and alkalinity conditions. Error bars represent standard deviation of measurements from duplicate experiments.

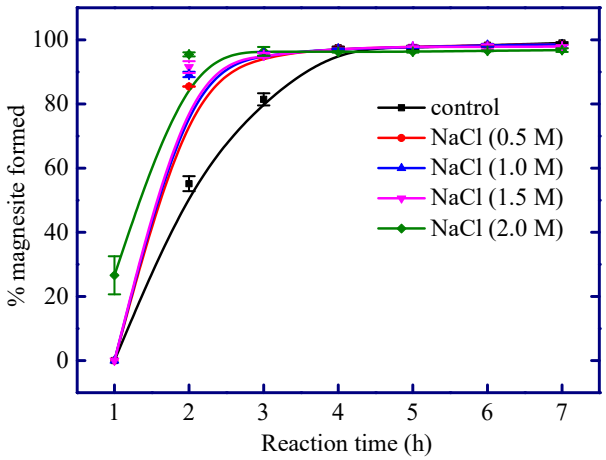

Fig. 6. Magnesite transformation reaction curves under background electrolyte environments.

3.3 MgO NANOPARTICLE EFFECTS

The solid MgO particles in the solution can act as a surface for nucleation and growth of carbonates. In MgO experiments, all peaks in the XRD patterns agree with hydromagnesite reference data at one hour reaction time (Fig. 7). This implies that hydromagnesite is preferentially precipitated in MgO experiments. At 2 hours reaction time, the transformed anhydrous magnesite in 6 mg MgO experiment ($0.127\pm7.6\times10^{-3}$ g) is kinetically inhibited compared to the control experiment ($0.180\pm5.6\times10^{-3}$ g) (Table A.1-2; Table A.15-16; Fig. 8 and 3a). Basis-splines (a spline function) were used for curve-fitting (Fig. 9). The systematically varied data of magnesite percentage with increasing MgO content seem fall within error of each other at two hours reaction

time (Fig. 9). However, the weight data confirm that the replacement of hydromagnesite to anhydrous magnesite is inhibited (the formed magnesite decreased from $0.127\pm7.6\times10^{-3}$ g to $0.099\pm1.5\times10^{-2}$) at two hours reaction time with an increase in the amount of MgO particles (from 6 mg to 24 mg) (Fig. 8 and 9). Furthermore, the average magnesite content of MgO experiments at three hours reaction time exceeds the average magnesite content of control experiments (Fig. 9Fig. 9). At three hours reaction time, the formed anhydrous magnesite in 6 mg MgO experiment ($0.340\pm3.9\times10^{-3}$ g) is facilitated compared to the control experiment ($0.279\pm6.6\times10^{-4}$ g) (Table A.1-2; Table A.15-16). Interestingly, brucite ($Mg(OH)_2$) content at the end of experiment is slightly higher than those obtained in the other experiments (e.g. control, acidity, alkalinity, and NaCl influenced experiments) (e.g. Table A.22). Additionally, the ultimately formed magnesite in MgO experiments ($0.376\pm2.8\times10^{-4}$ g in 24 mg MgO experiments) is higher than that in control experiments ($0.352\pm2.4\times10^{-3}$ g).

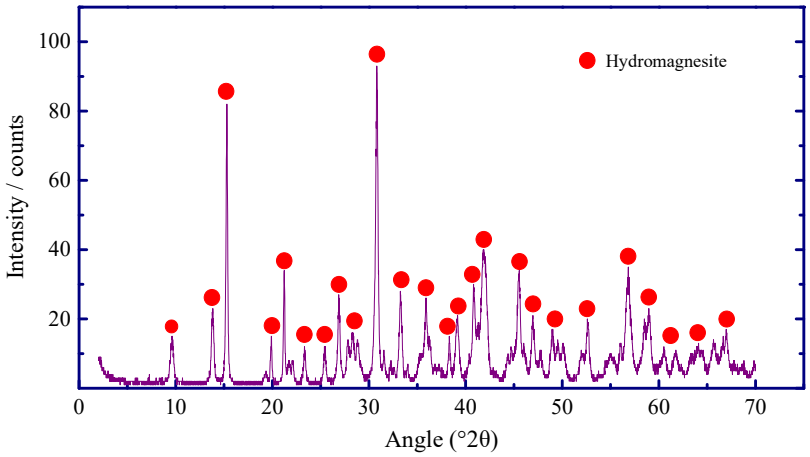

Fig. 7. X-ray diffractogram of reaction products in the 6 mg nano MgO experiment at one hour reaction time.

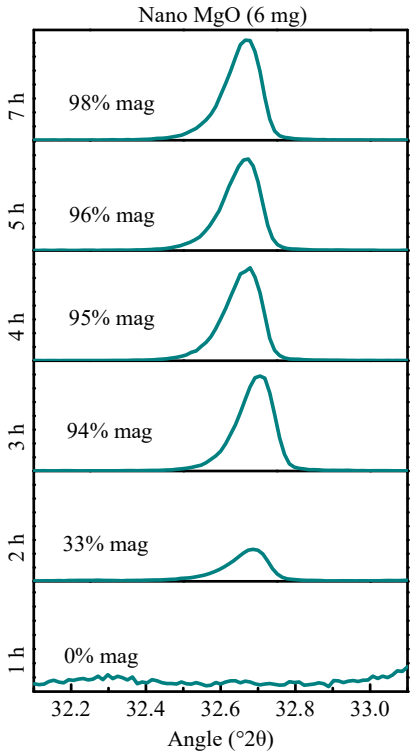

Fig. 8. Powder X-ray diffractogram of reaction products in the 6 mg MgO experiments (selected area from 32.1-33.1 °2θ).

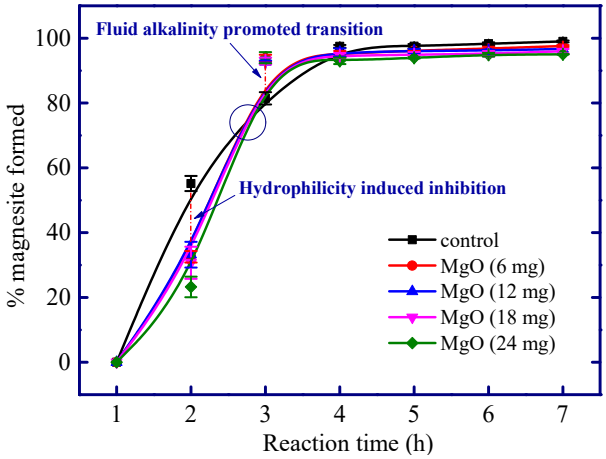

Fig. 9. Magnesite transformation reaction curves showing the effect of the addition of MgO.

4 Discussion

4.1 TRANSFORMATION MECHANISM OF MAGNESITE

Our results show that magnesite is formed as a result of replacement of hydromagnesite and oxymagnesite. The peculiar phase oxymagnesite has only been documented in a few previous studies, and it is considered to originate from the thermal decomposition of various hydrated magnesium carbonates such as nesquehonite ($MgCO_3 \cdot 3H_2O$) (above 373 K) (Eq. (1)) (Ballirano et al., 2010; Frykstrand et al., 2014). The formation of nesquehonite at room temperature is well known (Kloprogge et al., 2003; Cheng et al., 2009), and the formation of hydromagnesite can be expected at higher temperature (above 40 °C) (Zhang et al., 2006; Cheng and Li, 2009). A direct transformation of nesquehonite to hydromagnesite has been reported to occur at 353 K (around 80 °C) (Hao and Du, 2009). As discussed in Section 2.1, the fluids in our experiments were mixed at room temperature just prior to placing them in a pre-heated oven at 200 °C. Previous studies have already demonstrated that nesquehonite is commonly precipitated upon mixing $MgCl_2$ and Na_2CO_3 at room temperature (Kloprogge et al., 2003; Cheng and Li, 2009). Hence, at elevated temperature, replacement of nesquehonite by oxymagnesite and hydromagnesite through thermal decomposition (Eq. (1)) and direct transformation (Eq. (2)) (e.g. Wang et al., 2019) is the expected reaction pathway.

$$3(MgCO_3 \cdot 3H_2O) \rightarrow MgO \cdot 2MgCO_3 + CO_2 + 9H_2O \quad (1)$$

$$5(MgCO_3 \cdot 3H_2O) \rightarrow 4MgCO_3 \cdot Mg(OH)_2 \cdot 4H_2O + CO_2 + 10H_2O \quad (2)$$

According to the Ostwald step rule, the metastable phases are progressively substituted by more stable phases (Morse and Casey, 1988). Hence, it could be speculated that hydromagnesite and oxymagnesite are more easily crystallized than magnesite since these metastable magnesium carbonates can eventually be substituted by anhydrous magnesite over a certain length of time (Table A.1; Fig. 3a). The metastable hydrated magnesium carbonates serve as crystalline precursors and decrease the energy barrier for magnesite formation, and these intermediates may dehydrate and order prior to their crystallization to magnesite (Montes-Hernandez and Renard, 2016). Moreover, it has been reported that nesquehonite decomposition induced oxymagnesite (above 373 K) can ultimately produce magnesite in the temperature range 423-483 K (Ballirano et al., 2010). The temperature of 200 °C used in this study coincides with the reported temperature for oxymagnesite to magnesite replacement. Furthermore, it is noted that dehydration of hydromagnesite could induce the precipitation of magnesite (Zhang et al., 2000), and thus liberate water molecules in the hydromagnesite structure, resulting in the formation of magnesite and brucite (Eq. (3)). The identified trace of brucite (1% of $Mg(OH)_2$) at the end of experiment can support this interpretation (Table A.1). Additionally, the magnesite formation may also originate from the transition of hydromagnesite through solid-state transformation with carbonate ions (Eq. (4)) (e.g. Power et al., 2019).

$$4MgCO_3 \cdot Mg(OH)_2 \cdot 4H_2O \leftrightarrow 4MgCO_3 + Mg(OH)_2 + 4H_2O \quad (3)$$

$$4MgCO_3 \cdot Mg(OH)_2 \cdot 4H_2O + CO_3^{2-} \leftrightarrow 5MgCO_3 + 4H_2O + 2OH^- \quad (4)$$

4.2 EFFECT OF FLUID pH ON MAGNESITE FORMATION

Our experimental results show that H^+ ions can facilitate to a minor extent the formation of magnesite. It is highly plausible that H^+ ions inhibit magnesium carbonate formation and yield HCO_3^- ions in solution. Laboratory experiments have demonstrated that hydromagnesite can precipitate by heating Mg-HCO_3 aqueous solution above 100 °C (Alderman, 1965; Bethke, 1996; Tran et al., 2016). Given that the transformation of nesquehonite to oxymagnesite and hydromagnesite occurs at elevated temperature, hydromagnesite precipitation from Mg-HCO_3 solution is a possible reaction pathway that could increase the content of hydromagnesite. At one hour reaction time, our results confirm that the weight of hydromagnesite in the HCl experiments ($0.176 \pm 5.0 \times 10^{-4}$ g) is significantly higher than that in control experiments ($0.121 \pm 4.0 \times 10^{-3}$ g). Since the transformation of hydromagnesite into magnesite could release OH^- ions in

aqueous solution, a higher transformed weight of hydromagnesite could potentially lead to a more alkaline aqueous environment. From the first hour to the second hour of the reaction, the transformed weight of hydromagnesite in HCl experiments ($0.0907\pm1.3\times10^{-2}$ g) is higher compared to that in control experiments ($0.0596\pm2.6\times10^{-4}$ g) (Table A.1-4). Moreover, our results confirm that the pH in HCl experiments is higher than that in control experiments (Fig. 10), and this coincides with higher transformed weight of hydromagnesite. A higher pH environment raises CO_3^{2-} activity, thus further favouring the phase transition of hydromagnesite to anhydrous magnesite. Hence, a slight increase in magnesite content can be expected in 10^{-5} M HCl experiments compared to control experiments.

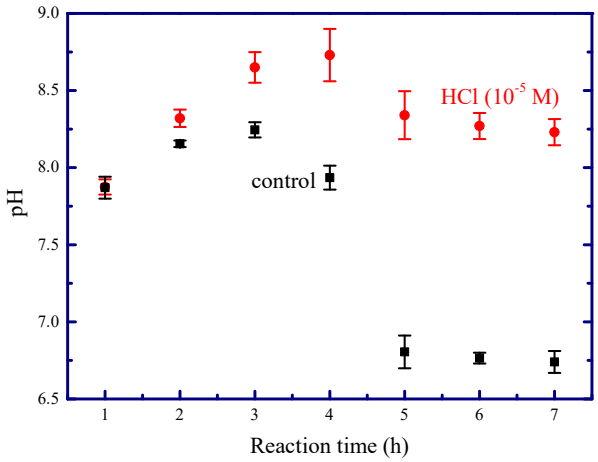

Fig. 10. pH variation during magnesite formation in control and HCl (10-5 M) experiments.

The hydroxyl ions may have a positive impact on hydromagnesite formation (Wang and Li, 2012). Our results confirm a higher weight of hydromagnesite in NaOH experiments ($0.170\pm1.0\times10^{-2}$ g) compared to control experiments ($0.121\pm4.0\times10^{-3}$ g) at one hour reaction time, thus verifying that NaOH can act as a catalyst and favour the production of hydromagnesite. Furthermore, addition of NaOH makes the fluid more alkaline, and our results demonstrate a higher pH in NaOH experiment compared to control experiments (Fig. 11). The predominance of carbonate ions over bicarbonate ions in an alkaline environment enhances hydromagnesite to magnesite replacement. In CO_2 (gas) to carbonate (solid) transformation experiments, it has been found that NaOH catalyses brucite carbonation and promotes magnesite formation due to the increased carbonate ion concentration (Montes-Hernandez et al., 2012). Li (2015) also indicates that higher pH can accelerate the transformation of hydromagnesite into magnesite in the presence of NaOH. A higher pH scenario favours the precipitation of carbonate minerals since CO_3^{2-} ions are most abundant at alkaline environments, and thus increases the saturation index of the fluid with respect to magnesite and also leads to a higher kinetic replacement of magnesite (Eq. (4)).

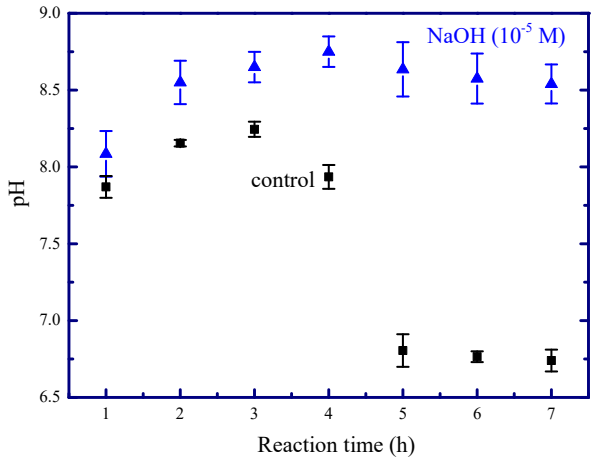

Fig. 11. pH variation during magnesite formation in control and NaOH (10-5 M) experiments.

4.3 EFFECT OF SALINE ENVIRONMENT (NaCl) ON MAGNESITE FORMATION

A saline environment interferes with the interaction between water molecules and magnesium ions and enhances dehydration of the magnesium ions because of decreased water activity (Christ and Hostetler, 1970), thus enhancing the nucleation of magnesite. The natural occurrence of authigenic magnesite is also associated with saline environments (Alderman and Von der Borch, 1961). Actually, hypersaline scenarios have been documented to favor the dehydration of hydromagnesite and the formation of magnesite crystallization (Zhang et al., 2000). Magnesium ions can form one of the strongest bonds with water molecules, resulting in $[Mg(H_2O)_6]^{2+}$ complexes. $[Mg(H_2O)_6]^{2+}$ complexes limit rapid formation of magnesite from aqueous fluids (Xu et al., 2013). However, $[Mg(H_2O)_6]^{2+}$ complexes are less stable in fluids of higher ionic strength, following the Debye-Hückel theory and extensions. Magnesium dehydration can be enhanced for magnesite formation as a result of Na^+ and other ions competing with Mg^{2+} for water molecules. In 2.0 M NaCl experiments, there are only about 10 water molecules available per ion according to our calculation (Vandeginste et al., 2019). Previous studies revealed that the inner hydration shell around Mg^{2+} contains 6 water molecules and the outer hydration shell is composed of 12 water molecules (18 water molecules could therefore attach to Mg^{2+} ions) (Pavlov et al., 1998; Markham et al., 2002). We speculate that a competition for hydration water could occur between the background ions and magnesite building ions, however, a slightly lesser extent could be expected for lower NaCl concentration experiments. Hence, a saline environment can facilitate magnesium dehydration and incorporation of magnesium into magnesite crystal. A high content of magnesite (27%) at one hour reaction time confirms this speculation (Fig. 5). Moreover, higher ionic strength induced catalytic effects on the dehydration of hydromagnesite is also a possible way that can accelerate magnesite formation (Sayles and Fyfe, 1973; Zhang et al., 2000), and this explains a higher transformed amount of hydromagnesite in NaCl experiments compared to control experiments (Section 3.2).

4.4 EFFECT OF MgO NANOPARTICLES ON MAGNESITE FORMATION

Higher brucite content in MgO experiments compared to the other experiments may be attributed to the hydrophilic nature of the MgO surface, which enables the ability to adsorb a single monolayer of water molecules at room temperature and results in the conversion of the uppermost MgO layers to a hydroxide structure (partial transformation) (Coluccia et al., 1988; Xu and Goodman, 1997; Foster et al., 2005). Moreover, brucite carbonation by interaction with carbonate ions is a possible reaction pathway that can increase the formation of magnesite. At the end of the experiments, assuming that the extra magnesite in 24 mg MgO experiments (compared to control experiments) comes from the hydration and carbonation of MgO particles, approximate 11.6 mg MgO is converted into magnesite, and this is a reasonable value for the used MgO in our experiments. Similarly, if the extra brucite in 24 mg MgO experiments (compared to control experiments) comes from the hydration of MgO particles, approximate 11.1 mg MgO is converted into brucite. This indicates

that the addition of MgO particles can increase the ultimate amount of the formed magnesite and brucite in MgO experiments.

MgO particles can act as nucleation sites for the precipitation of metastable magnesium carbonates. No brucite is detected at one or two hours reaction time (e.g. Table A.15-16), and this implies that the brucite (MgO hydration) at the uppermost MgO layers may gradually recrystallize and form hydromagnesite. The continuously increased weight of hydromagnesite (from $0.385\pm1.3\times10^{-3}$ g to $0.428\pm3.4\times10^{-3}$ g) with the addition of MgO (from 6 mg to 24 mg) at one hour reaction time confirm that more hydromagnesite may originate from the MgO particles. Our results show that the magnesite percentage is lower than that in control experiments at two hours reaction time, and the magnesite percentage decreases with adding the amount of MgO in solutions. This is ascribed to the fact that the water liberation process during the phase transition of the surface precipitated hydromagnesite to anhydrous magnesite is impeded since the hydrophilic nature of the MgO surface can lead to the strong interaction with water because of the formation of hydrogen bonds (water adsorption) (Tikhomirov and Jug, 2000) (Eq. (3)). This explains the lower content of magnesite in MgO experiments compared to control experiments at two hours reaction time. In contrast, hydrophobic activated carbon facilitate magnesite formation since the kinetics of the water-repellent process during hydromagnesite to magnesite replacement can be enhanced because of the hydrophobic nature of activated carbon (Atashin et al., 2017). Furthermore, the newly formed $Mg(OH)_{2(s)}$ may occur upon the continuous hydration of MgO particles. It has already been demonstrated that the MgO powder slurry has a high pH value and could provide alkaline pH environments (Sawai et al., 2000; Romero-Güiza et al., 2015). This may accelerate hydromagnesite to magnesite replacement by direct transformation since CO_3^{2-} ions are most abundant at alkaline environments (Eq. (4)). At three hours reaction time, our results confirm that the solution pH of MgO experiments is higher than the pH of control experiments (Fig. 12), and this can subsequently provide a favourable scenario for magnesite formation and can explain the higher magnesite content. Although MgO nanoparticles may retard the initial formation of magnesite, it is highly probable that an alkaline environment can subsequently facilitate the formation of magnesite by enhanced hydromagnesite to magnesite replacement.

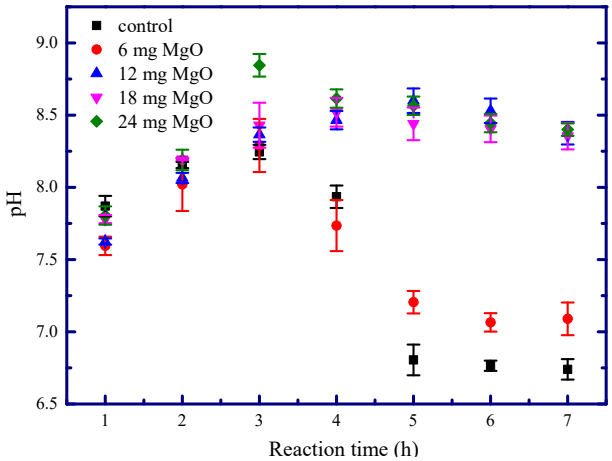

Fig. 12. pH variation during magnesite formation in control and MgO experiments.

5 Conclusions

The formation of acid-resistant precipitates that can effectively block carbon leakage mitigate risks involved with underground CO_2 storage and offer solutions for remediation (pore blocking). Hence, effective chemical solutions are investigated and tested to plug potential carbon leakage pathways by the formation of acid-resistant precipitates. Multiple batch reactor experiments were conducted to evaluate magnesite formation and the underlying geochemical processes at mineral-fluid interfaces with a range of fluid chemistries. We have documented the effect of fluid composition and complexity on the kinetics of replacement of metastable magnesium carbonates to magnesite. Fluid alkalinity accelerates magnesite formation by raised CO_3^{2-} activity. Magnesium dehydration can catalyse magnesite formation in saline environment. MgO hydration created alkaline environment favours magnesite formation. Hence, these results are critical for the practitioners to optimise the remediation fluids. The researchers and practitioners can consider several solutions for blockage of CO_2 leakage pathways, which may depend on local or environmental factors. Our main conclusions are:

(1) Slightly acidic fluid can facilitate to a minor extent the formation of magnesite. Higher conversion amount of hydromagnesite is observed in HCl experiments and this can potentially release more OH^- ions and raise the fluid pH, thus facilitating hydromagnesite to magnesite replacement. Fluid alkalinity can accelerate magnesite formation since an alkaline environment favours the transformation of hydromagnesite into magnesite because of the higher CO_3^{2-} activity.

(2) Magnesite formation is quicker in more saline fluids. The interaction between water molecules and magnesium ions is impacted by the presence of NaCl, and a competition for hydration water can occur between the background ions and magnesite building ions. This can facilitate magnesium dehydration and incorporation of magnesium into the magnesite crystal.

(3) MgO nanoparticles have a major influence on magnesite formation compared to seedless conditions (control experiments). MgO hydrophilicity retards magnesite formation at the initial stage since water liberation during the phase transition from hydromagnesite to magnesite is impeded because of the strong interaction of water with hydrophilic surfaces. An alkaline environment can subsequently accelerate magnesite formation by enhanced hydromagnesite to magnesite replacement.

Acknowledgments

This research was funded by the European Commission Horizon 2020 (grant number 764531) and KU Leuven Internal Funds Bijzonder Onderzoeksfonds 2020 (grant number STG/20/013). We would like to thank Stephen Argent for assistance with and maintenance of the powder X-ray diffractometer in the School of Chemistry, and Hannah Constantin for assistance with DIFFRAC. EVA-XRD software in Faculty of Engineering.

Appendix 1

Supplementary material:

Table A 1 Percentage of different minerals as a function of reaction time in control experiment (Relative mineral percentages are derived from PXRD analyses of the reaction products)

Time (hours)	Hydromagnesite (%)	Oxymagnesite (%)	Magnesite (%)	Brucite (%)	Total product mass (g)	pH
1	39.6	60.4	0	0	0.2991	7.92
2	18.2	24.9	56.8	0	0.3241	8.17
3	8.0	9.2	82.8	0	0.3361	8.21
4	0	0	97.8	2.2	0.3495	7.99
5	0	0	97.1	2.9	0.3540	6.88
6	0	0	98.0	2.0	0.3543	6.79
7	0	0	98.8	1.2	0.3545	6.69

Table A 2 Percentage of different minerals as a function of reaction time in control experiments (repeat)

Time (hours)	Hydromagnesite (%)	Oxymagnesite (%)	Magnesite (%)	Brucite (%)	Total product mass (g)	pH
1	40.8	59.2	0	0	0.304	7.82
2	19.5	26.9	53.5	0	0.3293	8.14
3	9.7	10.2	80.1	0	0.3486	8.28
4	0	0	97.2	2.8	0.3478	7.88
5	0	0	98.0	2.0	0.3527	6.73
6	0	0	98.6	1.4	0.3549	6.74
7	0	0	99.2	0.8	0.3565	6.79

Table A 3 Percentage of different minerals as a function of reaction time in 10^{-5} M HCl experiments

Time (hours)	Hydromagnesite (%)	Oxymagnesite (%)	Magnesite (%)	Brucite (%)	Total product mass (g)	pH
1	59.5	40.5	0	0	0.2954	7.84
2	28.9	12.1	59.0	0	0.3266	8.36
3	0	0	97.1	2.9	0.3461	8.72
4	0	0	97.8	2.2	0.3506	8.85
5	0	0	98.3	1.7	0.3537	8.45
6	0	0	98.3	1.7	0.3567	8.33
7	0	0	99.1	0.9	0.3608	8.29

Table A 4 **Percentage of different minerals as a function of reaction time in 10^{-5} M HCl experiments (repeat)**

Time (hours)	Hydromagnesite (%)	Oxymagnesite (%)	Magnesite (%)	Brucite (%)	Total product mass (g)	pH
1	58.3	41.7	0	0	0.3027	7.91
2	22.8	18.1	59.1	0	0.3357	8.28
3	0	3.6	96.0	0.4	0.3501	8.58
4	0	0	97.6	2.4	0.3528	8.61
5	0	0	98.3	1.7	0.3570	8.23
6	0	0	98.2	1.8	0.3606	8.21
7	0	0	98.1	1.9	0.3577	8.17

Table A 5 **Percentage of different minerals as a function of reaction time in 10^{-5} M NaOH experiments**

Time (hours)	Hydromagnesite (%)	Oxymagnesite (%)	Magnesite (%)	Brucite (%)	Total product mass (g)	pH
1	56.3	43.7	0	0	0.2902	8.19
2	11.0	0	87.1	1.9	0.3403	8.65
3	0	0	96.8	3.2	0.3306	8.72
4	0	0	97.1	2.9	0.3430	8.82
5	0	0	97.9	2.1	0.3604	8.76
6	0	0	97.2	2.8	0.3568	8.69
7	0	0	98.2	1.8	0.3603	8.63

Table A 6 **Percentage of different minerals as a function of reaction time in 10^{-5} M NaOH experiments (repeat)**

Time (hours)	Hydromagnesite (%)	Oxymagnesite (%)	Magnesite (%)	Brucite (%)	Total product mass (g)	pH
1	56.8	43.2	0	0	0.3125	7.98
2	17.1	0	80.6	2.3	0.3482	8.45
3	9.8	4.5	85.7	0	0.3582	8.58
4	0	0	89.7	3.0	0.3581	8.68
5	0	0	97.3	2.7	0.3572	8.51
6	0	0	98.4	1.6	0.3620	8.46
7	0	0	98.8	1.2	0.3569	8.45

Table A 7 **Percentage of different minerals as a function of reaction time in 0.5 M NaCl experiments**

Time (hours)	Hydromagnesite (%)	Oxymagnesite (%)	Magnesite (%)	Brucite (%)	Total product mass (g)	pH
1	47.8	52.2	0	0	0.2944	7.71
2	7.4	7.1	85.5	0	0.3458	8.29
3	0	0	94.7	5.3	0.3491	8.42
4	0	0	97.3	2.7	0.3595	8.33
5	0	0	98.2	1.8	0.3618	8.19
6	0	0	98.5	1.5	0.3614	8.11
7	0	0	98.7	1.3	0.3598	8.07

Table A 8 **Percentage of different minerals as a function of reaction time in 0.5 M NaCl experiments (repeat)**

Time (hours)	Hydromagnesite (%)	Oxymagnesite (%)	Magnesite (%)	Brucite (%)	Total product mass (g)	pH
1	49.7	50.3	0	0	0.2949	7.76
2	8.9	5.6	85.4	0	0.3451	8.33
3	0	0	95.9	4.1	0.3561	8.31
4	0	0	97.5	2.5	0.3586	8.25
5						
6	0	0	98.1	1.9	0.3631	8.02
7	0	0	98.7	1.3	0.3585	7.94

Table A 9 **Percentage of different minerals as a function of reaction time in 1.0 M NaCl experiments**

Time (hours)	Hydromagnesite (%)	Oxymagnesite (%)	Magnesite (%)	Brucite (%)	Total product mass (g)	pH
1	42.5	57.5	0	0	0.3062	7.69
2	0	5.7	89.8	4.4	0.3338	8.29
3	0	0	95.2	4.8	0.3531	8.54
4	0	0	97.3	2.7	0.3552	8.60
5	0	0	97.5	2.5	0.3524	8.58
6	0	0	98.0	2.0	0.3494	8.63
7	0	0	98.6	1.4	0.3598	8.55

Table A 10 **Percentage of different minerals as a function of reaction time in 1.0 M NaCl experiments (repeat)**

Time (hours)	Hydromagnesite (%)	Oxymagnesite (%)	Magnesite (%)	Brucite (%)	Total product mass (g)	pH
1	41.5	58.5	0	0	0.2969	7.77
2	0	7.2	88.6	4.2	0.3389	8.27
3	0	0	96.0	4.0	0.3509	8.52
4	0	0	97.0	3.0	0.3511	8.47
5	0	0	97.9	2.1	0.3603	8.53
6	0	0	98.6	1.4	0.3620	8.49
7	0	0	98.6	1.4	0.3600	8.40

Table A 11 **Percentage of different minerals as a function of reaction time in 1.5 M NaCl experiments**

Time (hours)	Hydromagnesite (%)	Oxymagnesite (%)	Magnesite (%)	Brucite (%)	Total product mass (g)	pH
1	43.5	56.5	0	0	0.3044	7.64
2	0	2.6	92.8	4.6	0.3390	8.24
3	0	0	94.6	5.4	0.3498	8.40
4	0	0	97.3	2.7	0.3550	8.50
5	0	0	97.8	2.2	0.3485	8.61
6	0	0	98.3	1.7	0.3525	8.46
7	0	0	98.2	1.8	0.3574	8.36

Table A 12 **Percentage of different minerals as a function of reaction time in 1.5 M NaCl experiments (repeat)**

Time (hours)	Hydromagnesite (%)	Oxymagnesite (%)	Magnesite (%)	Brucite (%)	Total product mass (g)	pH
1	54.2	45.8	0	0	0.3160	7.64
2	0	8.8	90.2	1.0	0.3443	8.21
3	0	0	95.7	4.3	0.3488	8.30
4	0	0	97.3	2.7	0.3587	8.38
5	0	0	97.9	2.1	0.3628	8.49
6	0	0	97.3	2.7	0.3589	8.42
7	0	0	97.6	2.4	0.3602	8.43

Table A 13 **Percentage of different minerals as a function of reaction time in 2.0 M NaCl experiments**

Time (hours)	Hydromagnesite (%)	Oxymagnesite (%)	Magnesite (%)	Brucite (%)	Total product mass (g)	pH
1	37.9	39.7	22.4	0	0.2966	7.53
2	0	0.7	95.0	4.4	0.3269	7.81
3	0	0	95.5	4.5	0.3174	7.87
4	0	0	96.1	3.9	0.3207	7.94
5	0	0	96.5	3.5	0.3120	7.95
6	0	0	96.7	3.3	0.3213	8.07
7	0	0	97.2	2.8	0.3363	8.09

Table A 14 **Percentage of different minerals as a function of reaction time in 2.0 M NaCl experiments (repeat)**

Time (hours)	Hydromagnesite (%)	Oxymagnesite (%)	Magnesite (%)	Brucite (%)	Total product mass (g)	pH
1	16.1	53.1	30.8	0	0.3080	7.54
2	0	0	95.9	4.1	0.3358	8.13
3	0	0	97.4	2.6	0.3478	8.16
4	0	0	96.4	3.6	0.3259	8.26
5	0	0	96.1	3.9	0.3229	8.31
6	0	0	96.5	3.5	0.3262	8.36
7	0	0	96.4	3.6	0.3405	8.39

Table A 15 **Percentage of different minerals as a function of reaction time in 6 mg nano MgO experiments**

Time (hours)	Hydromagnesite (%)	Oxymagnesite (%)	Magnesite (%)	Brucite (%)	Total product mass (g)	pH
1	100.0	0	0	0	0.3864	7.64
2	68.7	0	31.3	0	0.3878	7.89
3	0	0	93.1	6.9	0.3627	8.16
4	0	0	95.8	4.2	0.3664	7.86
5	0	0	96.3	3.7	0.3674	7.26
6	0	0	97.2	2.8	0.3722	7.11
7	0	0	97.4	2.6	0.3706	7.17

Table A 16 **Percentage of different minerals as a function of reaction time in 6 mg nano MgO experiments (repeat)**

Time (hours)	Hydromagnesite (%)	Oxymagnesite (%)	Magnesite (%)	Brucite (%)	Total product mass (g)	pH
1	100.0	0	0	0	0.3845	7.55
2	66.2	0	33.8	0	0.3908	8.15
3	0	0	94.6	5.4	0.3628	8.42
4	0	0	94.6	5.4	0.3644	7.61
5	0	0	96.0	4.0	0.3665	7.15
6	0	0	96.4	3.6	0.3663	7.02
7	0	0	97.8	2.2	0.3659	7.01

Table A 17 **Percentage of different minerals as a function of reaction time in 12 mg nano MgO experiments**

Time (hours)	Hydromagnesite (%)	Oxymagnesite (%)	Magnesite (%)	Brucite (%)	Total product mass (g)	pH
1	100.0	0	0	0	0.3999	7.64
2	69.6	0	30.4	0	0.4036	8.04
3	0	0	92.4	7.6	0.3728	8.40
4	0	0	94.7	5.3	0.3754	8.51
5	0	0	95.6	4.4	0.3763	8.66
6	0	0	96.0	4.0	0.3781	8.59
7	0	0	96.7	3.3	0.3777	8.43

Table A 18 **Percentage of different minerals as a function of reaction time in 12 mg nano MgO experiments (repeat)**

Time (hours)	Hydromagnesite (%)	Oxymagnesite (%)	Magnesite (%)	Brucite (%)	Total product mass (g)	pH
1	100.0	0	0	0	0.3937	7.61
2	64.0	0	36.0	0	0.4022	8.09
3	0	0	93.0	7.0	0.3757	8.33
4	0	0	96.5	3.5	0.3784	8.42
5	0	0	96.5	3.5	0.3791	8.54
6	0	0	96.4	3.6	0.3801	8.47
7	0	0	96.7	3.3	0.3794	8.32

Table A 19 **Percentage of different minerals as a function of reaction time in 18 mg nano MgO experiments**

Time (hours)	Hydromagnesite (%)	Oxymagnesite (%)	Magnesite (%)	Brucite (%)	Total product mass (g)	pH
1	100.0	0	0	0	0.4182	7.76
2	72.8	0	27.2	0	0.4198	8.20
3	0	0	93.7	6.3	0.3806	8.32
4	0	0	94.1	5.9	0.3808	8.45
5	0	0	94.3	5.7	0.3833	8.36
6	0	0	94.6	5.4	0.3837	8.34
7	0	0	95.5	4.5	0.3855	8.29

Table A 20 **Percentage of different minerals as a function of reaction time in 18 mg nano MgO experiments (repeat)**

Time (hours)	Hydromagnesite (%)	Oxymagnesite (%)	Magnesite (%)	Brucite (%)	Total product mass (g)	pH
1	100.0	0	0	0	0.4077	7.80
2	65.8	0	34.2	0	0.4159	8.19
3	0	0	92.2	7.8	0.3821	8.54
4	0	0	95.2	4.8	0.3851	8.59
5	0	0	95.5	4.5	0.3871	8.52
6	0	0	95.8	4.2	0.3852	8.47
7	0	0	96.5	3.5	0.3877	8.42

Table A 21 **Percentage of different minerals as a function of reaction time in 24 mg nano MgO experiments**

Time (hours)	Hydromagnesite (%)	Oxymagnesite (%)	Magnesite (%)	Brucite (%)	Total product mass (g)	pH
1	100.0	0	0	0	0.4254	7.76
2	79.0	0	21.0	0	0.4220	8.14
3	0	0	92.7	7.3	0.3853	8.79
4	0	0	92.3	7.7	0.3936	8.66
5	0	0	93.8	6.2	0.3936	8.61
6	0	0	95.3	4.7	0.3970	8.40
7	0	0	95.0	5.0	0.3958	8.37

Table A 22 **Percentage of different minerals as a function of reaction time in 24 mg nano MgO experiments (repeat)**

Time (hours)	Hydromagnesite (%)	Oxymagnesite (%)	Magnesite (%)	Brucite (%)	Total product mass (g)	pH
1	100.0	0	0	0	0.4302	7.85
2	74.5	0	25.5	0	0.4317	8.24
3	0	0	95.2	4.8	0.3843	8.90
4	0	0	93.7	6.3	0.3909	8.57
5	0	0	94.1	5.9	0.3904	8.52
6	0	0	94.5	5.5	0.3930	8.49
7	0	0	95.1	4.9	0.3958	8.43

Glossary

Milli-Q refers to water that has been purified using resin filters and deionized to a high degree by a water purification system manufactured by Millipore Corporation. The system monitors the ion concentration by measuring the electrical resistance of the water. Higher resistance means fewer charge carrying ions. It dispenses the water through a 0.22 µm membrane filter with a specific resistance of 18.2 micro-ohms. Pure and ultrapure water is available directly from tap water at a flow rate of 3 L/minute.

Web links:

www.che.iitb.ac.in/online/labfacility/milli-q-water-system

6 References

Alderman, A.R., Von der Borch, C.C., 1961. Occurrence of magnesite-dolomite sediments in South Australia. Nature 192, 861.

Alderman, A.R., 1965. Dolomite sediments and their environment in the southeast of South Australia. Geochim Cosmochim Acta 29, 1355-1365

Allnér, O., Nilsson, L., Villa, A., 2012. Magnesium ion-water coordination and exchange in biomolecular simulations. J Chem Theory Comput 8, 1493-1502.

Atashin, S., Varin, R.A., Wen, J.Z., 2017. Directed precipitation of anhydrous magnesite for improved performance of mineral carbonation of CO_2. J Environ Chem Eng 5, 3362-3372.

Bethke, C., 1996. Geochemical reaction modelling: Concepts and applications. Oxford University Press, New York, USA, 397 p.

Benson, S.M., Hepple, R., Apps, J., Tsang, C.F., Lippmann, M.J., 2002. Lessons learned from natural and industrial analogues for storage of carbon dioxide in deep geological formations. Lawrence Berkeley National Laboratory Report LBNL 51170.

Braissant, O., Decho, A.W., Dupraz, C., Glunk, C., Przekop, K.M., 2007. Exopolymeric substances of sulfate-reducing bacteria: Interactions with calcium at alkaline pH and implication for formation of carbonate minerals. Geobiology 5, 401-411.

Ballirano, P., De Vito, C., Ferrini, V., Mignardi, S., 2010. The thermal behaviour and structural stability of nesquehonite, $MgCO_3 \cdot 3H_2O$, evaluated by in situ laboratory parallel-beam X-ray powder diffraction: New constraints on CO2 sequestration within minerals. J Hazard Mater 178, 522-528.

Bracco, J.N., Stack, A.G., Higgins, S.R., 2014. Magnesite step growth rates as a function of the aqueous magnesium: carbonate ratio. Cryst Growth Des 14, 6033-6040.

Brydie, J.R., Perkins, E.H., Fisher, D., Girard, M., Valencia, M., Olson, M., Rattray, T., 2014. The development of a leak remediation technology for potential non-wellbore related leaks from CO_2 storage site. Energy Procedia 63, 4601-4611.

Christ, C.L., Hostetler, P.B., 1970. Studies in the system $MgO\text{-}SiO_2\text{-}CO_2\text{-}H_2O$ (II): The activity product constant of magnesite. Am J Sci 268, 439-453.

Coluccia, S., Lavagnino, S., Marchese, L., 1988. The hydroxylated surface of MgO powders and the formation of surface sites. Mater Chem Phys 18, 445-464.

Cheng, W., Li, Z., George, P.D., 2009. Effects of temperature on the preparation of magnesium carbonate hydrates by reaction of $MgCl_2$ with Na_2CO_3. Chin J Chem Eng 17, 661-666.

Cheng, W., Li, Z., 2009. Precipitation of nesquehonite from homogeneous supersaturated. Res Technol 44, 937-947.

Castaneda-Herrera, C.A., Stevens, G.W., Haese, R.R., 2018. Review of CO_2 leakage mitigation and remediation technologies. Geological Carbon Storage: Subsurface Seals and Caprock Integrity, 238, p. 327.

Deelman, J.C., 2001. Breaking Ostwald's rule. Chemie der Erde 61, 224-235.

Foster, M., D'Agostino, M., Passno, D., 2005. Water on MgO(100)-an infrared study at ambient temperatures. Surf Sci 590, 31-41.

Frykstrand, S., Strietzel, C., Forsgren, J., Ångström, J., Potin, V., Strømme, M., 2014. Synthesis, electron microscopy and X-ray characterization of oxymagnesite, $MgO{\cdot}2MgCO_3$, formed from amorphous magnesium carbonate. CrystEngComm 16, 10837-10844.

Hänchen, M., Prigiobbe, V., Baciocchi, R., Mazzotti, M., 2008. Precipitation in the Mg-carbonate system-effects of temperature and CO_2 pressure. Chem Eng Sci 63, 1012-1028.

Hao, Z., Du, F., 2009. Synthesis of basic magnesium carbonate microrods with a "house of cards" surface structure using rod-like particle template. J Phys Chem Solids 70, 401-404.

Ito, T., Kawamura, Y., Sekine, K., Hayashi, K., 2006. Laboratory study of trapping enhancement by the in-situ reaction method for geological storage of CO_2. In: Proc. of the 8th International Conference on Greenhouse Gas Control Technologies, June 19-22, Trondheim, Norway (CD-ROM).

Ito, T., Xu, T., Tanaka, H., Taniuchi, Y., Okamoto, A., 2014. Possibility to remedy CO_2 leakage from geological reservoir using CO_2 reactive grout. Int J Greenh Gas Con 20, 310-323.

Königsberger, E., Königsberger, L.C., Gamsjäger, H., 1999. Low-temperature thermodynamic model for the system Na_2CO_3-$MgCO_3$-$CaCO_3$-H_2O. Geochim Cosmochim Acta 63, 3105-3119.

Kaszuba, J.P., Janecky, D.R., Snow, M.G., 2003. Carbon dioxide reaction processes in a model brine aquifer at 200 °C and 200 bars: implications for geologic sequestration of carbon. Appl Geochem 18, 1065-1080.

Kloprogge, J.T., Martens, W.N., Nothdurft, L., 2003. Low temperature synthesis and characterisation of nesquehonite. J Mater Sci Lett 22, 825-829.

Kim, J., Yu, S., Yun, S., Kim, K., Kim, J., Shinn, Y., Chae, G., 2019. CO_2 leakage detection in the near-surface above natural CO_2-rich water aquifer using soil gas monitoring. Int J Greenh Gas Con 88, 261-271.

Tran, K.T., Han, K.S., Kim, S.J., Kim, M.J., Tran, T., 2016. Recovery of magnesium from Uyuni salar brine as hydrated magnesium carbonate. Hydrometallurgy 160, 106-114.

Lackner, K.S., 2003. A guide to CO_2 sequestration. Science 300, 1677-1678.

Lions, J., Devau, N., de Lary, L., Dupraz, S., Parmentier, M., Gombert, P., Dictor, M.C., 2014. Potential impacts of leakage from CO_2 geological storage on geochemical processes controlling fresh groundwater quality: a review. Int J Greenh Gas Con 22, 165-175.

Li, C., 2015. The Preparation and Flame-retardant Properties of magnesite (MgCO3). MSc Thesis (In Chinese), Zhengzhou University, Zhengzhou, China.

Morse, J.W., Casey, W.H., 1988. Ostwald process and mineral paragenesis in sediments. Am J Sci 288, 537-560.

Markham, G.D., Glusker, J.P., Bock, C.W., 2002. The arrangement of first- and second-sphere water molecules in divalent magnesium complexes: results from molecular orbital and density functional theory and from structural crystallography. J Phys Chem B 106, 5118-5134.

Montes-Hernandez, G., Rrnard, F., Chiriac, R., Findling, N., Toche, F., 2012. Rapid Precipitation of Magnesite Microcrystals from $Mg(OH)_2$-H_2O-CO_2 Slurry Enhanced by NaOH and a Heat-Aging Step (from ~20 to 90 °C). Cryst Growth Des 12, 5233-5240.

Montes-Hernandez, G., Renard, F., 2016. Time-resolved in situ raman spectroscopy of the nucleation and growth of siderite, magnesite, and calcite and their precursors. Cryst Growth Des 16, 7218-7230.

Mosleh, M. H., Govindan, R., Shi, J.Q., Durucan, S., Korre, A., 2017. The use of polymer-gel remediation for CO2 leakage through faults and fractures in the caprock. Energy Procedia 114, 4164-4171.

Pavlov, M., Siegbahn, P.E.M., Sandström, M., 1998. Hydration of beryllium, magnesium, calcium, and zinc ions using density functional theory. J Phys Chem A 102, 219-228.

Palandri, J.L., Kharaka, Y.K., 2004. A compilation of rate parameters of water-mineral interaction kinetics for application to geochemical modelling. U. S. Geological Survey. Open File Report.

Pokrovski, O.S., Golubev, S.V., Schott, J., Castillo, A., 2009. Calcite, dolomite and magnesite dissolution kinetics in aqueous solutions at acid to circumneutral pH, 25 to 150 °C and 1 to 55 atm pCO_2: New constraints on CO_2 sequestration in sedimentary basins. Chem Geol 265, 20-32.

Power, I.M., Harrison, A.L., Dipple, G.M., Wilson, S.A., Kelemen, P.B., Hitch, M., Southam, G., 2013. Carbon mineralization: From natural analogues to engineered systems. Rev Mineral Geochem 77, 305-360.

Power, I.M., Harrison, A.L., Dipple, G.M., Wilson, S.A., Barker, S.L.L., Fallon, S.J., 2019. Magnesite formation in playa environments near Atlin,British Columbia, Canada. Geochim Cosmochim Acta 255, 1-24.

Romero-Güiza, M.S., Tait, S., Astals, S., del Valle-Zermeño, R., Martínez, M., Mata-Alvarez, J., Chimenos, J.M., 2015. Reagent use efficiency with removal of nitrogen from pig slurry via struvite: A study on magnesium oxide and related by-products. Water Res 84, 286-294.

Sayles, F., Fyfe, W., 1973. The crystallization of magnesite from aqueous solution. Geochim Cosmochim Acta 37 (1), 87-99.

Sawai, J., Kojima, H., Igarashi, H., Hashimoto, A., Shoji, S., Sawaki, T., Hakoda, A., Kawada, E., Kokugan, T., Shimizu, M., 2000. Antibacterial characteristics of magnesium oxide powder. World J Microb Biot 16, 187-194.

Sear, R.P., 2006. Heterogeneous and homogeneous nucleation compared: rapid nucleation on microscopic impurities. J Phys Chem B 110(10), 4985-4989.

Saldi, G. D., Jordan, G., Schott, J., Oelkers, E.H., 2009. Magnesite growth rates as a function of temperature and saturation state. Geochim Cosmochim Acta 73(19), 5646-5657.

Swanson, E.J., Fricker, K.J., Sun, M., Park, A., 2014. Directed precipitation of hydrated and anhydrous magnesium carbonates for carbon storage. Phys Chem Chem Phys 16, 23440.

Thompson, J.B., Ferris, F.G., 1990. Cyanobacterial precipitation of gypsum, calcite, and magnesite from natural alkaline lake water. Geology 18, 995-998.

Tikhomirov, V.A., Jug, K., 2000. MSINDO study of water adsorption on the clean MgO(100) surface. J Phys Chem B 104, 7619-7622.

Valdiya, K.S., 1968. Origin of the magnesite deposits of southern Pithoragarh, Kumaun Himalaya, India. Econ Geol 63, 924-934.

Vandeginste, V., Snell, O., Hall, M.R., Steer, E., Vandeginste, A., 2019. Acceleration of dolomitization by zinc in saline waters. Nat Commun 10, 1851.

Wang, D., Li, Z., 2012. Gas-liquid reactive crystallization kinetics of hydromagnesite in the $MgCl_2$−CO_2−NH_3−H_2O system: Its potential in CO_2 sequestration. Ind Eng Chem Res 51, 16299-16310.

Wang, Y., Yin, W., Li, C., Yuan, Z., 2019. Synthesis and kinetic analysis of hydromagnesite with different morphologies by nesquehonite method. Indian J Chem Technol 26, 514-521.

Xu, C., Goodman, D.W., 1997. Structure and geometry of water adsorbed on the MgO (100) surface. Chem Phys Lett 265, 341-346.

Xu, J., Yan, C., Zhang, F., Konishi, H., Xu, H., Teng, H.H., 2013. Testing the cation-hydration effect on the crystallization of Ca-Mg-CO3 systems. Proc Natl Acad Sci USA 110, 17750-17755.

Yang, Y., Sahai, N., Romanek, C.S., Chakraborty, S., 2012. A computational study of Mg^{2+} dehydration in aqueous solution in the presence of HS^- and other monovalent anions - insights to dolomite formation. Geochim Cosmochim Acta 88, 77-87.

Zhang, P., Anderson, H.L., Kelly, J.W., Krumhansl, J.L., Papenguth, H.W., 2000. Kinetics and mechanisms of formation of magnesite from hydromagnesite in brine. Technical Report SAN099-19465, Sandia National Laboratories, Albuquerque, NM 87185-0750, USA.

Zhang, Z., Zheng, Y., Ni, Y., Liu, Z., Chen, J., Liang, X., 2006. Temperature- and pH-dependent morphology and FTIR analysis of magnesium carbonate hydrates. J Phys Chem B 110, 12969-12973.